10414–10425 *Nucleic Acids Research, 2013, Vol. 41, No. 22* *Published online 11 September 2013*
doi:10.1093/nar/gkt792

Dissecting the oligonucleotide binding properties of a disordered chaperone protein using surface plasmon resonance

Mireille Baltzinger[1], Kamal Kant Sharma[2], Yves Mély[2] and Danièle Altschuh[1,*]

[1]Biotechnologie et signalisation cellulaire, Université de Strasbourg, CNRS, BP10413, 67412 Illkirch, France and [2]Laboratoire de Biophotonique et Pharmacologie, UMR 7213 CNRS, Faculté de Pharmacie, Université de Strasbourg, 67401, Illkirch, France

Received July 11, 2013; Revised August 8, 2013; Accepted August 9, 2013

ABSTRACT

We have used surface plasmon resonance to investigate the nucleic acid binding properties of the core protein of hepatitis C virus, a disordered protein believed to chaperone the genomic RNA. It was previously shown that a peptide (peptide E) corresponding to the association of two basic clusters of core enhances the annealing and the dimerization of nucleic acid fragments derived from a stem loop (SL2) in the 3′ untranslated region of the hepatitis C virus genome. However, strong aggregation of nucleic acids by core or peptide E in the excess of the latter precluded the characterization of their binding parameters up to now. By careful design of surface plasmon resonance experiments, we obtained accurate binding parameters for the interaction of peptide E with SL2-derived oligonucleotides of different lengths and sequences, in form of stem-loop, duplex or strand. Peptide E was found to bind in a salt dependent manner to all oligonucleotides assayed. Affinity data identify at least two binding modes, of which one is independent of sequence/structure, and the other is specific to the SL2 stem-loop fold. Stoichiometry data support a multi-motif binding model allowing formation of higher-order complexes. We propose that the modular binding mode demonstrated for structured RNA-binding proteins also applies to this disordered chaperone and is relevant to its activity.

INTRODUCTION

Hepatitis C virus (HCV) is an enveloped, single-stranded, positive-sense RNA virus that belongs to the Flaviviridae family and causes liver diseases worldwide. Its 9.6 kb genome contains a single open reading frame flanked by 5′ and 3′ untranslated regions (UTRs) that play essential roles in RNA replication and translation. Post-translational cleavage of the polyprotein encoded by the HCV genome yields 10 viral proteins, among which is the nucleocapsid protein, named core [for review (1–3)]. The mature core is a protein of ~21 kDa with multiple functions in the viral life cycle. Its highly basic and hydrophilic N-terminal domain was shown to bind nucleic acids as well as a number of host and cellular proteins. Its C-terminal hydrophobic domain mediates interactions with lipids and membrane proteins [for review (4–7)].

This work focuses on the RNA-binding properties of the N-terminal part of core as measured by surface plasmon resonance (SPR). Core is believed to bind RNA and act as a chaperone, a function also displayed by the core proteins of other Flaviviridae (8). Indeed, *in vitro* experiments have shown that core facilitates structural rearrangements of the 3′-UTR of the HCV genome, leading to RNA dimerization (9,10). Core is also able to enhance the annealing of complementary HIV- or HCV-derived DNA and RNA sequences (9,11,12). Although little information is available on the structural and molecular aspects of core-RNA interactions in capsid assembly, the *in vitro* analysis of its chaperone properties has identified nucleic acid fragments with lengths between 16 and 27 nt that are re-structured and therefore presumably recognized by core. The aim of our study was to investigate whether it is possible to identify and quantify distinct RNA-core binding modes, potentially related to its different functions. For this purpose, SPR measurements were performed with the molecules used for investigating chaperone activities (10,12) (Table 1). We used a peptide named peptide E, corresponding to the association of two of the three basic clusters of the N-terminal domain of core (BD2 and BD3) and shown to support the dimerization and annealing activities (10–12) (Figure 1). The RNA fragments were derived from the sequence of the second stem loop (SL2), predicted in one of the possible conformations of the X-region of the 3′UTR HCV genome (10).

*To whom correspondence should be addressed. Tel: +33 3 68 85 48 32; Fax: +33 3 68 85 46 83; Email: daniele.altschuh@unistra.fr

Table 1. Oligonucleotides (ONs) used in this study

Name	ON sequence	MW	Length (nt)
	deoxy-ON		
dDLS	5′biotin-TCACGGCTAGCTGTGA-3′	5302	16
dPal2	5′-T**G**ACG**C**CTAGCTGTGA-3′biotin	5467	16
dPal2	5′biotin-T**G**ACG**C**CTAGCTGTGA-3′	5302	16
dRD	5′biotin-T**GC**CG**CG**TAG**A**TGT**AC**-3′	5302	16
d(TG)4	5′-TGTGTGTG-3′biotin	3041	8
	ribo-ON		
DLS	5′-UCACGGCUAGCUGUGA-3′biotin	5666	16
Pal2	5′-U**G**ACG**C**CUAGCUGUGA-3′biotin	5666	16
DLSloop	5′-UCACGGCU**UU**CUGUGA-3′biotin	5604	16
cDLS	5′-UCACAGCUAGCCGUGA-3′biotin	5650	16
Half-DLS	5′-AGCUGUGA-3′biotin	3119	8
duplex DLS-DLS	5′-UCACGGCUAGCUGUGA-3′biotin 3′biotin-AGUGUCGAUCGGCACU-5′	11332	16 × 2
duplex DLS-dDLS	5′-TCACGGCTAGCTGTGA-3′ 3′biotin-AGUGUCGAUCGGCACU	10536	16 × 2
duplex DLS-cDLS	5′-UCACGGCUAGCUGUGA-3′biotin 3′biotin-AGUGCCGAUCGACACU-5′	11315	16 × 2
SL2	5′-UCACGGCUAGCUGUGAAAGGUCCGUGA-3′biotin	9258	27
SL2stem	5′-**AG**ACGGCUAGCUGUGAAAGGUCCGU**CU**-3′biotin	9258	27
SL2loop	5′-UCACGGCUAGCUGUG**UUU**GGUCCGUGA-3′biotin	9189	27
duplex SL2-cSL2	5′-UCACGGCUAGCUGUGAAAGGUCCGUGA-3′biotin 3′-AGUGCCGAUCGACACUUUCCAGGCACU-5′	17826	27 × 2

The bases that are substituted in the native sequence are marked in bold. The differences in base pairing between the three DLS duplexes are underlined. MW, molecular weight; nt, nucleotides.

Quantitative experimental investigation of protein–nucleic acid interactions is challenging because specific and non-specific binding events may co-exist and be of similar affinity. Although non-specific protein–protein interactions are unwanted, non-specific protein–nucleic acid binding is likely to be an important component of the recognition process, e.g. by facilitating the search for specific sites, a phenomenon amply studied in the case of DNA (13–15). Non-specific recognition can also be requested for nucleic acid coating in viral assembly. A relatively indiscriminate binding mode was also suggested to be one of two possible mechanisms for chaperoning RNA folding (16). In the first mechanism, the protein recognizes and stabilizes a specific RNA conformation required in the folding pathway. In the second, misfolded intermediates are destabilized by weak non-specific interactions, mainly due to electrostatic attraction between the positively charged amino acids of the chaperone and the negatively charged phosphates of the RNA backbone. To physically separate specific and non-specific sites on small RNA fragments in an attempt to isolate distinct binding modes is unrealistic. Binding may depend on structural features that are not necessarily preserved in short fragments. Larger fragments on the other hand provide opportunities for various folds and for co-existing binding modes that complicate data interpretation, but better account for biologically relevant recognition processes.

We expect to observe non-specific binding in the interaction system studied here, as peptide E is strongly positively charged (pI = 12.5, 18 Arg and 3 Lys in 59 residues; Figure 1). Furthermore, the N-terminal half of HCV core is believed to be disordered, which favors a non-discriminatory binding mode (17,18). Disorder, often found in chaperone proteins, was proposed to contribute to recognition diversity by facilitating their adaptation to various nucleic acid sequences and structures (19,20). Several activities of core may nevertheless rely on the preferential recognition of well-defined RNA sequence/structure elements. In particular, the analysis of HCV RNA dimerization in the presence of peptide E suggested that it is mediated by a 16 nt long palindromic sequence called dimer linkage sequence (DLS) located within SL2, and that the RNA sequence and structure influence the core-mediated dimerization (10,21). The palindromic DLS sequence in its stem-loop and duplex forms, together with mutants thereof that are unable to dimerize (Figure 1), represent a simple model to investigate whether peptide E discriminates between oligonucleotides (ONs) in stem-loop, duplex and unfolded forms. The larger SL2 stem loop used in annealing experiments (12) was included in our study because it contains structural features not present in DLS (Figure 1) that could provide other core recognition motifs.

In addition to challenges inherent to protein–nucleic acid binding, peptide E was found to aggregate in the presence of ONs, thus preventing binding studies by most solution assays. Surface methods represent a promising informative alternative because one of the partners is fixed so that events subsequent to the binding

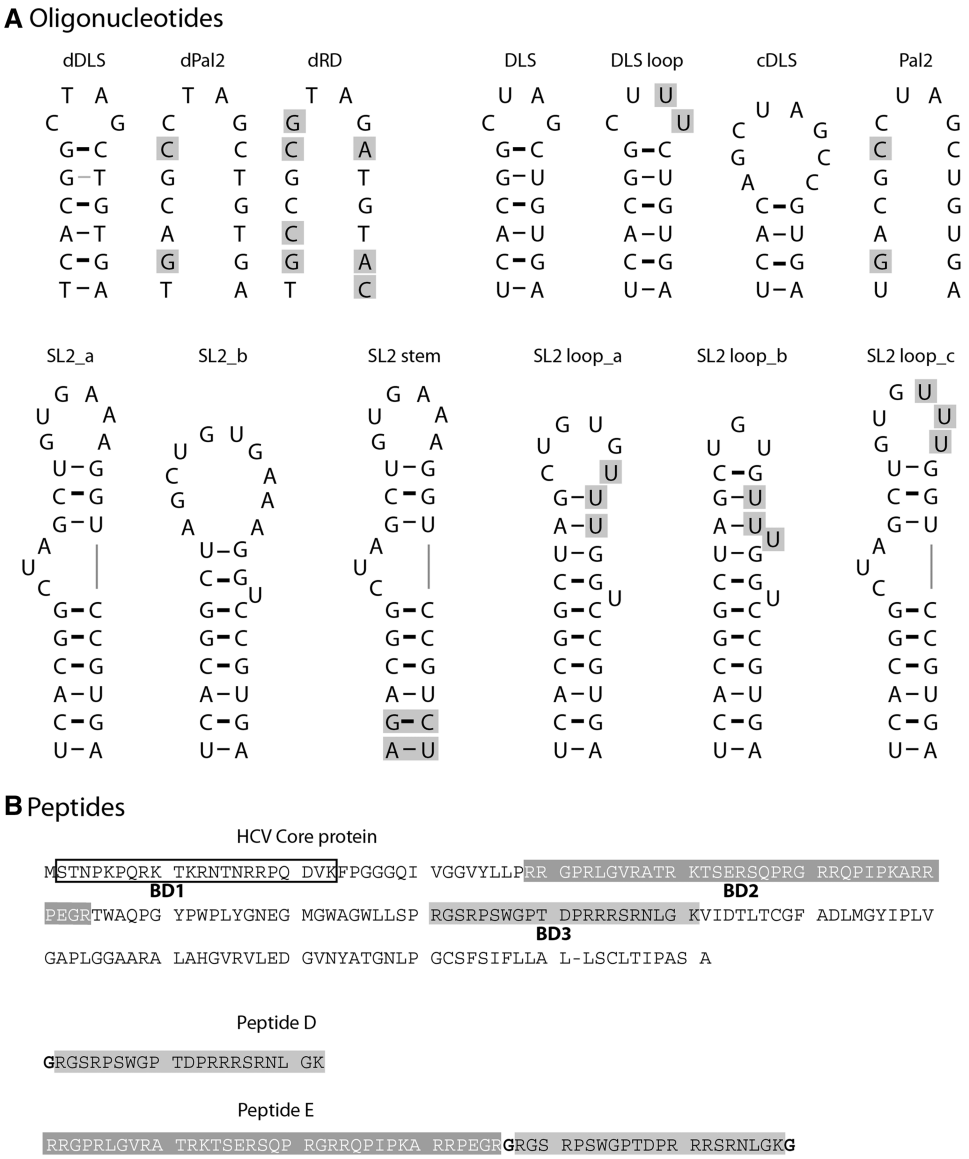

Figure 1. Oligonucleotide structures (**A**) and peptide sequences (**B**). (A) Secondary structures of the 16mer DLS derivatives (upper row) and the 27mer SL2 derivatives (lower row) were predicted with the Unafold Web Server program (http://mfold.rna.albany.edu/). The substituted positions in the variants are boxed in grey. The 2–3 most stable configurations predicted for SL2 (SL2_a,b) and SL2loop (SL2loop_a,b,c) are shown. (B) Primary sequences of the mature HCV core, peptide D (MW 2494 Da) and Peptide E (MW 6754 Da). The three basic domains of the N-terminal region of core (BD1, BD2 and BD3) are boxed.

step may be prevented. SPR represents a powerful approach to investigate protein–nucleic acid recognition (22–24). Binding is recorded in real time, and the resulting kinetic curves provide information not only on kinetics and affinity but also on the binding heterogeneity. Furthermore SPR responses are related to the mass of molecules at the sensor surface, thus giving access to stoichiometry information (25–27). Our data showed that peptide E bound, in a salt dependent manner, to all ONs assayed, irrespective of their fold and sequence. At 150 mM NaCl, its affinity (K_D) for most ONs was in the range of 0.1–0.4 μM. The heterogeneous kinetics and K_D around 50 nM observed with SL2 suggest the existence of a different, sequence/structure specific binding mode. Stoichiometries ranged from 0.7 to 2.7 peptide E/ON and were related with ON length, indicating that the peptide tends to coat the ONs. Analysis of the size-stoichiometry correlation led us to propose a multi-motif binding model in which two peptide E motifs bind two motifs located on the same or on different ONs.

MATERIALS AND METHODS

CM4 sensor chips and Biacore consumables were obtained from GE Healthcare. Streptavidin (ref S4762) was purchased from Sigma.

ONs and core peptides

The (3′ or 5′)-biotinylated ONs were purchased from IBA GmbH Nucleic Acids product Supply (Gottingen,

Germany) and Eurogentec S.A. (Liege, Belgium) and purified by the manufacturers by reverse phase high performance liquid chromatography. Their names and sequences are listed in Table 1. Peptides E and D were synthesized by solid phase peptide synthesis as described in (11). Their sequences are shown in Figure 1.

Biosensor experiments

All SPR experiments were performed with a Biacore 2000® instrument (GE-Healthcare Biacore, Uppsala, Sweden). The running buffer (HEPES-buffered saline, HBS) composition was 10 mM Hepes (pH 7.4), 150 mM NaCl, 3.4 mM EDTA, 0.005% P20 surfactant. (3′- or 5′-) labelled biotin-ONs (Table 1) were immobilized on streptavidin-coated CM4 sensor chips. CM4 sensor chips were preconditioned by duplicate injections of 10 mM HCl, 50 mM NaOH, 0.1% (w/v) SDS, each with a contact time of 10 s, and water with a contact time of 20 s. Before covalent immobilization of streptavidin, traces of biotinylated products that could remain in the flow system were neutralized by injecting a streptavidin solution (0.1 mg/ml in HBS) for 5–6 min through all flow cells. Streptavidin was then immobilized using standard amine-coupling methods. The surface was activated with a mixture of 0.5 mM 1-ethyl-3 -(3-dimethylaminopropyl) carbodiimide hydrochloride and 0.2 mM N-hydroxysuccinimide for 7 min, followed by a 6 min injection of streptavidin at 10–100 μg/ml in 10 mM sodium acetate (pH 5) and then blocked with 1 M ethylenediamine hydrochloride (pH 8.5) (instead of ethanolamine hydrochloride) for 7 min. Finally, the surface was subjected to four pulses (100 μl) of 1 M NaCl, 50 mM NaOH at a flow rate 50 μl/min to wash out all non-covalently bound streptavidin. This coupling method resulted in a density of 2000–3000 resonance units (RU) of streptavidin on all four flow cells. Before immobilization, the single-strand ONs, diluted at a low concentration of 10 nM in HBS, were heated at 90°C for 1 min and put on ice before injection onto the streptavidin-coated chip at 10 μl/min at 25°C to generate a 10–30 RU ON surface. ON duplexes were preformed by mixing equimolar quantities at high concentrations (≥25 μM in HBS) of the two ONs (except for the duplex DLS-DLS where 50 μM of DLS were used), heating the mix at 90°C for 1 min and then allowing it to reach slowly room temperature. In the case of SL2-cSL2, DLS-dDLS, the non-biotinylated ON was added in 20% excess. A dilution at 10 nM of the duplexes was used for injection onto the streptavidin-coated chip to reach a density ≤45 RU. Peptides were serially diluted in HBS (containing 0.01% P20 surfactant and NaCl as specified) to the final concentrations indicated in Figures 2 and 3 and injected at a flow rate of 50 μl/min for 1 min. The responses were also monitored during a 3-min dissociation phase. Although most binding experiments were characterized by a fast dissociation, the surfaces were systematically treated, after the 3-min dissociation step, with 0.1% SDS followed by 1 M NaCl in water, each for 30 s, to remove any residual protein. Each concentration series was run in duplicate (and partially in triplicate or quadruplicate). All binding data were collected at 25°C.

Data processing and steady-state analysis

Data processing and analysis was performed using Scrubber2 (BioLogic Software Pty Ltd; biologic.com.au). The responses were double-referenced (28) by subtracting from the signal on the ON surface, both the signal recorded on the reference surface (streptavidin without ON) and the signal of a blank injection with running buffer. The steady-state values were plotted against the peptide concentration. The K_D values were determined by non-linear regression analysis of the steady-state values using a single site model: $[ON.Pep] = R_{max\text{-}exp} \times [Pep]/(K_D + [Pep])$, where $R_{max\text{-}exp}$ is the maximal binding capacity, [ON.Pep], the concentration of complex at steady state, [Pep] the concentration of the free peptide and K_D, the equilibrium dissociation constant.

The binding stoichiometry was calculated as the ratio of experimental to theoretical maximal responses (25–27). The experimental maximal response, $R_{max\text{-}exp}$ (SPR response achieved when the immobilized binder is saturated with the injected binder), was fitted from affinity data. The theoretical maximal response, $R_{max\text{-}theor}$, can be calculated because the SPR signal is directly related to the mass of molecules at the sensor surface. $R_{max\text{-}theor}$ was predicted for a one:one binding mode (each ON molecule binds one peptide E molecule): $R_{max\text{-}theor} = MW_{Pep} \times RU_{ON}/MW_{ON}$, where MW_{Pep}, MW_{ON} are the molecular weights of peptide and ON, respectively, and RU_{ON} the SPR signal corresponding to the amount of immobilized ON. The binding stoichiometry was expressed as number of peptide molecules bound per ON ($St_{Pep/ON}$) or as number of nucleotides bound per peptide ($St_{nt/Pep}$). $St_{Pep/ON} = R_{max\text{-}exp}/R_{max\text{-}theor}$; $St_{nt/Pep}$ = total number of nucleotides (in ON)/$St_{Pep/ON}$.

The distance between two ONs in the dextran matrix was calculated as follows. The surface density (RU) is related to the mass/mm^2 by the relation 1 RU = 1 pg/mm^2 and was translated into a volume density (mass/vol) assuming a thickness of 100 nm of the dextran layer. The number of molecules/vol is calculated assuming a homogeneous distribution. This allows to estimate the volume of the cube that contains one molecule: $(MW_{ON} \times 10^6)/(RU_{ON} \times 6)$ Å^3 and therefore the distance between two ONs [see also (26)].

RESULTS

Deoxy-ON binding properties of peptide E

We first optimized the conditions of SPR experiments using deoxy-ONs instead of ribo-ONs. To investigate whether peptide E is able to discriminate between deoxy-ONs with different folds, we compared its interaction with dDLS and with two variants thereof, in which the palindrome is disrupted: dPal2 and a random sequence called dRD. Their sequences and folds are shown in Table 1 and Figure 1, respectively. Initially, the peptide was immobilized on the sensor surface by amine coupling and flushed with the ON. This assay design should prevent potential peptide aggregation and allow the analysis of various ONs on a same peptide surface.

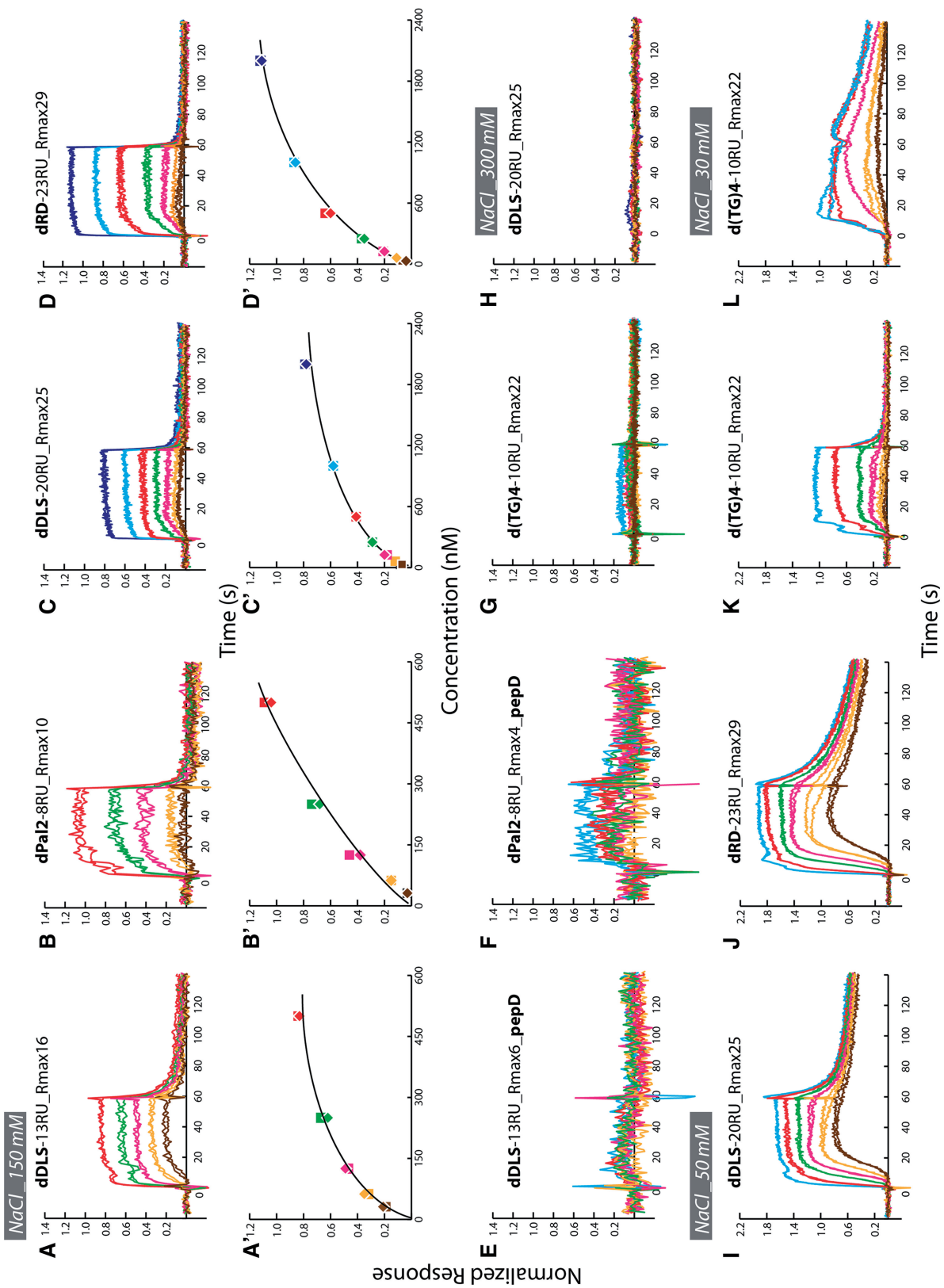

Figure 2. Typical sets of SPR binding curves and equilibrium fits for the interaction of peptides E and D with deoxy-ONs. The name of the ONs, together with their capture levels (RU) and expected saturation responses ($R_{max\text{-}theor}$) for 1:1 binding, are indicated above each set of curves. All experiments were performed with peptide E, except in E and F (peptide D as indicated). Binding was analysed at NaCl concentrations 150 mM (A–G), 300 mM (H), 50 mM (I–K) or 30 mM (L). Increasing concentrations of peptide solutions were injected for 60 s over the surfaces, followed by a 180 s flow of running buffer: 31 nM (brown), 62.5 nM (yellow), 125 nM (magenta), 250 nM (green), 500 nM (red), 1 μM (blue) and 2 μM (dark blue). Replicates, performed for each injection, are shown. To facilitate the comparison of binding levels, responses were normalized with respect to the theoretical maximum signal ($R_{max\text{-}theor}$) for 1:1 binding. The equilibrium responses, recorded 20 or 30 s after peptide injection, were plotted as a function of peptide E concentration (A'–D'). Binding parameters calculated from the fit to a 1:1 binding isotherm are listed in Table 2.

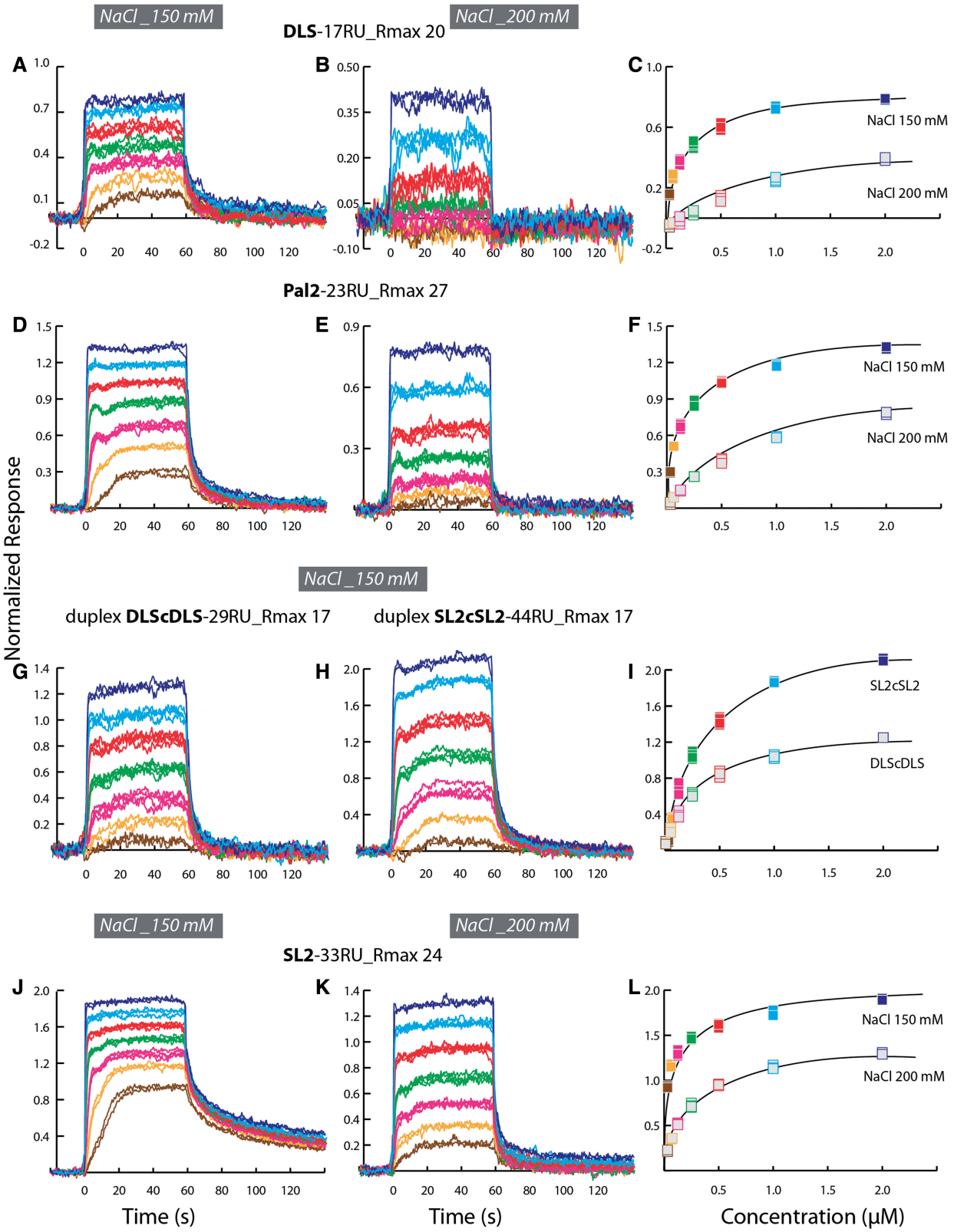

Figure 3. Typical sets of SPR binding curves and equilibrium fits for the interaction of peptide E with ribo-ONs. The name of the ONs, together with their capture levels (RU) and expected saturation responses ($R_{max\text{-}theor}$) for 1:1 binding, are indicated above each set of curves. Experiments were performed at 150 (A, D, G, H and J) or 200 (B, E and K) mM NaCl. The colour code is as in Figure 2. The concentration series of peptide E solutions were injected over the surfaces in duplicate or quadruplicate. The equilibrium fits corresponding to data shown in the left and central panels are shown in the right-hand panels (C, F, I and L), and resulting binding parameters are listed in Table 3.

However, binding was only observed at a relatively high peptide E density (≥300 RU) and at suboptimal salt concentration for carboxymethyldextran sensor surfaces ([NaCl] ≤ 50 mM). No affinity parameters could be determined owing to complex kinetic profiles and to progressive loss of binding activity during repetitive cycling. In contrast, when the deoxy-ONs were immobilized (by biotin-streptavidin capture) and flushed with peptide E, highly reproducible sensorgrams that allowed steady-state determination of K_D were obtained at low deoxy-ONs density ($R_{max} \leq 30$ RU) in the presence of 150 mM NaCl, after double-referencing of the data. We tested with dPal2 that the capture performed by their 3′ or 5′ ends generated similar responses. Typical sets of SPR binding curves are shown in Figure 2A–D. The K_D and stoichiometry ($St_{Pep/ON}$) values derived from fits of the equilibrium response versus peptide E concentration (Figure 2A′–D′) are reported in Table 2. The peptide was found to bind to the stem-loop dDLS with an equilibrium affinity (K_D) of 0.2 μM and a stoichiometry ($St_{Pep/ON}$) of 0.9 peptide/ON, and to the single stranded dPal2 and dRD with a 4–6-fold weaker affinity (0.9–1.2 μM) and 2-fold higher stoichiometry (2–2.2 peptides/ON). The binding parameters measured for dDLS and its variants thus indicate that peptide E interacts differently with the stem-loop dDLS as compared with the single-strands dPal2 and dRD.

We also recorded binding curves using the shorter peptide D that corresponds to the basic domain 3 (BD3) of core, or using deoxy-ON fragments unrelated to the SL2 sequence. At 150 mM NaCl, binding of peptide D to dDLS was undetectable (Figure 2E), and the signal observed on dPal2 (Figure 2F) and dRD (not shown) surfaces was weak. No or little binding was detected when peptide E was injected over surfaces containing the shorter deoxy-ONs d(TG)4 (Figure 2G) and d(A)8 (not shown), which may result from their small size or their sequence unrelated to DLS.

In an attempt to evaluate the electrostatic contribution to complex formation, binding experiments were performed in the NaCl 300 to 30 mM concentration range. No binding of peptide E to dDLS could be detected at 300 mM NaCl (Figure 2H). At 100 mM NaCl, the post-injection phases indicated a slightly slower dissociation (not shown), a phenomenon amplified at 50 mM NaCl (Figure 2I and J, Table 2). Binding curves at the lowest salt concentrations follow complex kinetics. Nevertheless, equilibrium values indicate a higher complex stability with decreasing [NaCl] (Table 2). Stoichiometry increases with decreasing salt in the case of dDLS but not dRD so that differences in binding properties between the stem-loop dDLS and the single-strand dRD become undetectable. Furthermore, binding was also detected at low salt concentration when peptide E was injected over d(TG)4 (Figure 2K and L: 50 and 30 mM NaCl, respectively) and d(A)8 surfaces, or when peptide D was injected over a dDLS surface (not shown). Thus, the salt-dependence of binding indicates a strong electrostatic contribution, as expected for the interaction between ONs and a positively charged peptide.

Table 2. Equilibrium parameters of peptide E binding to deoxy-ONs

Name	K_D (μM)	Stoichiometry		Number of replicates
		Peptide/ON $St_{Pep/ON}$	Nucleotides/peptide $St_{nt/Pep}$	
	NaCl 150 mM			
dDLS	0.24 ± 0.05	0.9 ± 0.1	17 ± 3	12
dPal2[a]	0.9 ± 0.3	2.2 ± 0.2	7 ± 1	5
dRD	1.2 ± 0.4	2.0 ± 0.6	8 ± 2	4
d(TG)4	Not detectable			
	NaCl 50 mM			
dDLS[b]	0.04	1.6	10	1
dRD[b]	0.04	1.9	8	1
d(TG)4[a]	1.1	2.2	4	1

[a]The binding parameters cannot be precisely evaluated because the highest peptide E concentration used is below $10 \times K_D$.
[b]In 25 mM Tris–HCl (pH 8) instead of 10 mM Hepes (pH 7.5).
K_D values were calculated by non-linear regression analysis of the data in Figure 2A′-D′ (and Supplementary Figures S1 and S2) using the Langmuir binding model. The standard deviations were calculated on the mean from ≥4 replicates. The stoichiometry ($St_{pep/ON}$) was obtained from the ratio $R_{max\text{-}exp}/R_{max\text{-}theor}$.

Binding of peptide E to DLS and its variants

Having optimized experimental conditions using deoxy-ONs, we analysed the binding of peptide E to the corresponding ribo-ONs. Because differences in peptide E binding to deoxy-ONs were most visible at 150 mM NaCl as compared with [NaCl] < 150 mM, and because binding was undetectable at 300 mM NaCl, the experiments with ribo-ONs were performed at 150 and 200 mM NaCl.

Eight DLS-derived ribo-ONs were assayed (Table 1): the wild-type DLS, Pal2 (carrying two replacements in the stem), DLSloop (carrying two replacements in the loop), the complementary sequence cDLS and three duplexes: DLS with itself (duplex DLS-DLS), with dDLS (duplex DLS-dDLS) and with cDLS (duplex DLS-cDLS). An 8mer corresponding to half of the DLS sequence (half-DLS) was also assayed.

Typical binding curves recorded with DLS and Pal2 at 150 and 200 mM NaCl are shown in Figure 3A, B, D and E, and the corresponding fits in Figure 3C and F (see also Supplementary Figures S1 and S2). Binding parameters are reported in Table 3. Binding curves typical of DLS-derived duplexes are shown in Figure 3G. Peptide E was observed to bind all of these 16mer ribo-ONs with similar affinities (K_D = 0.2–0.4 μM). This differs from what has been observed with the deoxy-ONs: peptide E bound dDLS with a 4–6-fold stronger affinity compared with dPal2 and dRD (Table 2). A lower affinity was measured for half-DLS (K_D = 3.1 μM). Stoichiometries were variable with a trend similar to that observed with 16mer deoxy-ONs: less peptide was bound to the stem-loops ($St_{Pep/ON}$ ~1 for DLS and dDLS), as compared with the strands Pal2, dPal2 and dRD ($St_{Pep/NA}$ between 1.5 and 2). The variant stem-loops DLSloop and cDLS showed stoichiometries of ~1.5 and 0.7, respectively. The

Table 3. Equilibrium parameters of peptide E binding to ribo-ONs

Name	K_D (μM)	Stoichiometry		Number of replicates
		Peptide/ON $St_{pep/ON}$	Nucleotides/peptide $St_{nt/pep}$	
	NaCl 150 mM			
DLS	0.20 ± 0.06	1.0 ± 0.2	17 ± 3	10
Pal2	0.19 ± 0.08	1.5 ± 0.1	11 ± 1	5
DLSloop	0.44 ± 0.10	1.4 ± 0.1	11 ± 1	5
cDLS	0.25 ± 0.02	0.7 ± 0.03	24 ± 1	3
Half DLS[a]	3.1 ± 0.1	0.9 ± 0.2	10 ± 2	4
duplex DLS-DLS	0.16 ± 0.03	1.6 ± 0.04	21 ± 0.5	2
duplex DLS-dDLS	0.17 ± 0.05	1.5 ± 0.05	21 ± 0.7	2
duplex DLS-cDLS	0.29 ± 0.05	1.4 ± 0.01	23 ± 0.1	2
duplex SL2-cSL2	0.33 ± 0.05	2.7 ± 0.3	20 ± 2	2
SL2	0.05 ± 0.01	1.8 ± 0.2	16 ± 2	9
SL2stem	0.05 ± 0.01	1.7 ± 0.1	16 ± 1	2
SL2loop	0.05 ± 0.01	1.6 ± 0.1	17 ± 1	2
	NaCl 200 mM			
DLS[a]	2.1 ± 0.2	0.9 ± 0.02	18 ± 1	2
Pal2[a]	1.5 ± 1.1	1.2 ± 0.2	13 ± 2	3
DLSloop[a]	2.7	1.0	17	1
cDLS[a]	4.9	0.8	20	1
duplex SL2-cSL2[a]	4.3	2.2	25	1
SL2	0.24 ± 0.19	1.3 ± 0.1	20 ± 1	7
SL2stem	0.34 ± 0.05	1.3 ± 0.01	20 ± 0.1	2
SL2loop	0.38 ± 0.14	1.2 ± 0.1	23 ± 1	2

[a]The binding parameters cannot be precisely evaluated because the highest peptide E concentration used is below $10 \times K_D$.
K_D values were calculated by a non linear regression analysis of the steady-state data (see Figure 3 C, F, I, L and Supplementary Figures S1 and S2), assuming a Langmuir binding model. The standard deviation was calculated on the mean for the number of replicates indicated in the last column.

responses were found to be specific to peptide E, as no binding signal was observed in the presence of non-related basic polypeptides such as K14R (sequence KRTAM FQDPQERPR; pI = 10.7), scFvQ34S (29) (pI = 10) or lysozyme (pI = 9.2) at similar concentrations (not shown). Binding parameters measured at 200 mM NaCl are also reported in Table 3. In line with a strong contribution of electrostatic interactions, equilibrium affinities were found to be about one order of magnitude lower at 200 mM compared with 150 mM NaCl (see also Supplementary Figure S2). Kinetic fits are reported in Supplementary Figures S1 and S2 and the resulting binding parameters in Supplementary Table S1. The K_D determined kinetically as k_{off}/k_{on} was found to be in good agreement with the K_D value evaluated from equilibrium responses reported in Table 3. Binding stoichiometries were either unaffected or slightly decreased by the increase in salt concentration.

Binding of peptide E to SL2 and its variants

We then investigated the interaction of peptide E with the 27mer SL2 and two SL2 variants with replacements in the stem (SL2stem) and loop (SL2loop) used in annealing experiments (12). SL2 and its variants are predicted to adopt various folds, of which the most stable, denoted a, b or c, are shown in Figure 1. SL2 was also used in the form of a duplex with its complementary strand (duplex SL2-cSL2, Table 1). Binding parameters are reported in Table 3, and illustrative sets of curves are shown in Figure 3H (for the duplex at NaCl 150 mM), and J andK (for SL2 at 150 and 200 mM NaCl, respectively). The corresponding equilibrium fits are shown in Figure 3I and L (and Supplementary Figures S1 and S2). The interaction strength between peptide E and the SL2-cSL2 duplex was similar to that of the shorter DLS duplexes (0.3 μM), but with a higher stoichiometry (compare Figure 3G and 3H). In contrast, SL2 showed a 4-fold stronger equilibrium affinity (K_D = 0.05 μM) compared with that of DLS (K_D = 0.2 μM). The kinetics at 150 mM NaCl (Figure 3J) were complex, resembling those observed with dDLS or dRD at 50 mM NaCl (Figure 2I and J). An evaluation of the equilibrium data using a two-site binding model yielded a high affinity component, with parameters close to those obtained with the simple Langmuir model (K_D = 0.03 μM; $St_{Pep/ON}$ = 1.4) and a poorly defined (~μM) low affinity component (not shown). No attempt was made to further analyse the binding curves because the conformational heterogeneity of SL2, also mentioned by Palau *et al.* (30), precluded the study of structure-binding relations. Affinity and stoichiometry parameters for peptide E interacting with the variants SL2stem and SL2loop (Langmuir binding model) were comparable with those observed with SL2. The SL2stem was not expected to behave differently from SL2. The similar K_Ds measured with SL2 and SL2loop indicates that the loop predicted in SL2 is not the sole determinant of strong binding. Binding parameters are influenced by the salt concentration, as observed for DLS and its variants.

DISCUSSION

Our aim was to investigate for the first time the ON binding properties and determinants of peptide E, a peptide encompassing two of the three basic domains of the HCV core protein and showing strong nucleic acid chaperone properties. The inherent disorder of the N-terminal end of HCV core complicates structural studies and its tendency to aggregate in the presence of ONs impedes binding studies in solution. Thus, we have used a surface-based approach to analyse the interaction of peptide E with ONs. Peptide E was shown previously to increase the dimerization of DLS (10) and the annealing of DLS, SL2 and SL2 variants with the corresponding complementary sequences (12). If these stem-loop structures present features that support specific recognition, their binding properties to peptide E should be different from those of strands and duplexes. We carefully designed and optimized SPR experiments to obtain precise affinity and stoichiometry parameters for the interaction of peptide E with ONs of different lengths and sequences derived from the SL2 sequence. Our data show that peptide E was able to recognize all ONs analysed. We searched for relationships between sequence/fold and the binding parameters recorded at 150 mM NaCl, for which the largest number of measurements was available.

Affinity and kinetics of the peptide E–ON interactions

A histogram representation of K_D values obtained at 150 mM NaCl for ONs classified according to their size within a given fold (strand, duplex and stem-loop) is shown in Figure 4A. No absolute correlation can be found between the K_D values and ON size. The 27mer stem-loops showed stronger peptide E binding (K_D ~50 nM) compared with the smaller 16mer stem-loops (K_D ~0.2–0.4 μM), and the 16mer strands stronger binding than the shorter 8mer strand (half-DLS), but the 16 and 27mer duplexes displayed similar peptide E binding in the 0.2–0.3 μM range. Also, the three 16mer strands (Pal2, dPal2, dRD) behaved differently, with up to 6-fold differences in K_D. A correlation between affinity and ON form is also not obvious. The 27mers in stem-loop form showed a stronger peptide E affinity (SL2, SL2loop, SL2stem: K_D ~50 nM) compared with the 27mer in duplex form (SL2-cSL2: K_D ~0.2 μM), but all 16mers, whether in stem-loop (DLS, dDLS, cDLS, DLSloop), duplex (DLS-DLS, DLS-dDLS, DLS-cDLS) or strand (Pal2) form, showed similar K_Ds in the 0.2–0.4 μM range at 150 mM NaCl.

The stronger equilibrium affinity measured for the interaction of peptide E with the 27mer stem-loops (SL2, SL2stem, SL2loop) likely represents a specific binding mode, supported by sequence/structure features not present in the SL2-cSL2 duplex or in the other ONs. The shape of the kinetic curves for the peptide E – SL2 interaction (Figure 3J) reflects complexities that prevent reliable mathematical fitting. The initial binding rates tend to be constant, as typically seen when limited by mass transport. Simulations (not shown) indicate that substantial mass transport cannot be achieved at the low ON densities used, when considering the binding

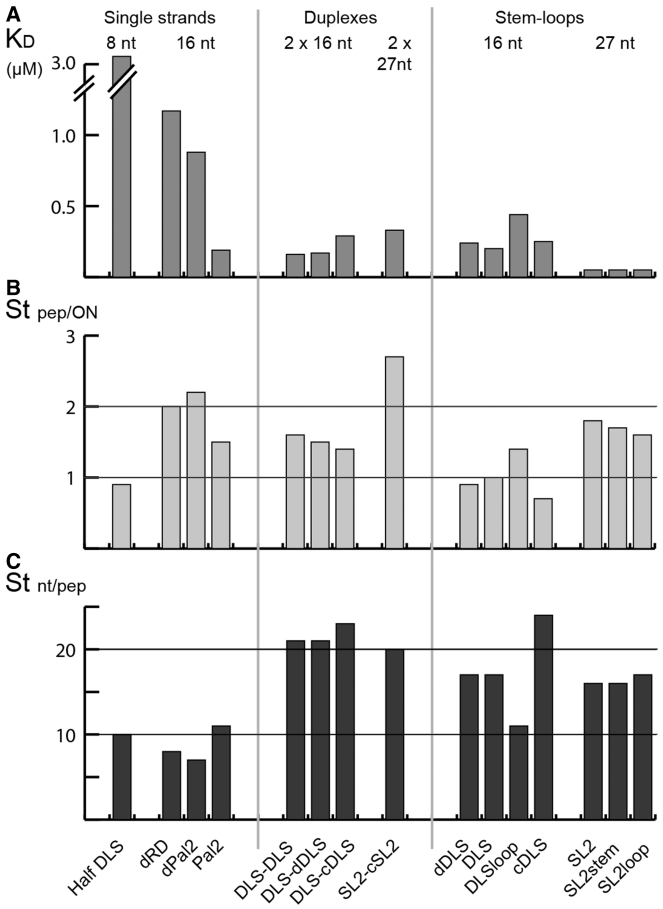

Figure 4. Relationship between the ON structure and its binding parameters to peptide E. The affinity (**A**), stoichiometry expressed as $St_{Pep/ON}$ (**B**) or $St_{nt/Pep}$ (**C**) are represented as histograms for each group of ON form (strands, duplexes, stem-loops) classified in order of increasing size.

parameters (K_D and saturation response, R_{max}) observed at equilibrium. A possible interpretation of the kinetic curves is that peptide E initially recognizes a few nucleotides (high density of small sites) with fast on-rates, before re-organizing into the complexes found at equilibrium that involve more nucleotides (low density of larger sites). Little selectivity and fast kinetics allow the sampling of a large number of configurations, which may be relevant in facilitating specific binding or in maximizing nucleic acid coating. The binding curves for the peptide E–SL2 interactions indicate multiple successive and/or co-existing events that appear to include a distinct, strong-affinity binding mode not observed with other ONs, most likely promoted by bulges or loops.

Most other ONs showed similar K_Ds in the 0.2–0.4 μM range at 150 mM NaCl. The higher K_D measured with half-DLS, dPal2 and dRD (1–3 μM range) could not be evaluated with high accuracy because equilibrium responses at the highest concentrations used are sometimes far away from surface saturation. Nevertheless, their peptide E binding affinity is clearly weaker than that measured with other ONs. This could be explained by the smaller size of half-DLS or by the difference in chemical structure between deoxy- and ribo-nucleotides

and will be discussed further later in the text. The similar K_Ds measured at 150 mM NaCl for ONs with different folds, together with the salt dependence of binding and stoichiometries above one (see later in the text), suggest a non-selective, electrostatically driven, binding mode. It is reasonable to assume that positive charges of peptide E (pI = 12.5) recognize ON backbone phosphates in a sequence and structure-independent manner.

Stoichiometry of the peptide E–ON interactions

In contrast to K_D values, the binding stoichiometry ($St_{Pep/ON}$) was related to ON size. A histogram representation of $St_{Pep/ON}$ for ONs classified according to their size within a given fold (strands, stem-loops and duplexes) is shown in Figure 4B. The number of peptide E molecules bound per ON increased with their length within each group of ON conformers. This observation suggests that peptide E occupies a defined surface on the ONs, irrespective of their sequence. The number of nucleotides statistically occupied ($St_{nt/Pep}$; column « Stoichiometry: Nucleotides/peptide » in Tables 2 and 3) was calculated by dividing the length of the ON by $St_{Pep/ON}$ (i.e. if one peptide binds to a 16mer, a maximum of 16 nt are needed for binding; if two peptides bind to a 16mer, a maximum of 8 nt are needed for binding). $St_{nt/Pep}$ is an alternative expression of stoichiometry that is independent of the ON size. Stoichiometries ($St_{Pep/ON}$, $St_{nt/Pep}$) are calculated assuming that the surface-fixed ONs are all capable of binding the peptide. It is well known that the covalent coupling of proteins can lead to their partial inactivation and that, at high densities, a fraction of the proteins may become inaccessible to the injected binding partner. Small synthetic molecules that are coupled in an oriented manner tend to be fully active, as observed by us for synthetic peptide binders (data not shown). The ONs captured on streptavidin surfaces through a terminal biotin are likely to be fully active and accessible, particularly at the very low coupling densities used here. This hypothesis is supported by the observation that similar $St_{nt/Pep}$ values were found for surfaces with different ON density and for ONs with different lengths (e.g. all duplexes). A second assumption is that the refractive index increment for proteins and nucleic acids is the same, as found by Di Primo and Lebars (31), who also summarized the divergent conclusions published by others. Whatever the exact relationship between RU and mass of nucleic acid at the sensor surface, the stoichiometries can be ranked and compared.

The histogram representation of $St_{nt/Pep}$ (Figure 4C) indicates that the number of nucleotides statistically occupied is relatively constant within each group, but differs across groups: 7–11, 20–23 and 16–17 nt are needed for peptide E binding to strands, duplexes and stem-loops, respectively. The two exceptions within stem-loops are the variants DLSloop and cDLS that differ from DLS in loop sequence and size, respectively. These exceptions hint to different mechanisms of complex formation with the native and non-native 16mer stem-loops, and to a possible sequence/structure-dependent binding, despite similar affinities. Within strands, the smaller $St_{nt/Pep}$ measured for deoxy- compared with ribo-ON strands (7–8 and 11 nt, respectively) can tentatively be related to the larger distance between consecutive phosphate groups in extended DNA (6.9 Å) as compared with extended RNA (5.5 Å). The theoretical extended lengths of a 8-nt deoxy- and a 11-nt ribo-ON are similar (55 and 60 Å, respectively) and could correspond to the surface occupied by peptide E. The relationship between size and stoichiometry suggests that peptide E tends to coat the ONs.

Model of peptide E interaction with strands and duplexes

The known overall structure of strands and duplexes allows speculating on the topology of regions occupied by the peptide. The stoichiometry ($St_{Pep/ON}$) of 1.5 peptide/ON calculated for Pal2 and DLS-derived duplexes (Table 3) could indicate the coexistence of different types of complexes on the sensor surface (i.e. mixture of 1:1 and 2:1 complexes), or the presence of a fraction of inactive or inaccessible ON. However, such phenomena are not expected to be systematically reproducible and are thus in variance with the highly reproducible value of 1.5 Pep/ON consistently measured for Pal2 (5 measurements) and for the three 16mer duplexes (1.5, 1.6, 1.4 in duplicate measurements). This stoichiometry can be interpreted as the formation of higher-order complexes containing three peptides and two ONs. The simplest model allowing the formation of such complexes requires 2 and 3 binding motifs on peptide E and the ONs, respectively: two motifs in peptide E could then coat two ON motifs, located on the same or on different ONs. The size of the ON motif covered by each peptide motif can be deduced from $St_{nt/Pep}$. In case of Pal2, $St_{nt/Pep}$ is ~11 nt. Each peptide motif would in this case cover 5–6 nt. The observation that peptide E needs twice as many nucleotides to bind 16mer duplexes ($St_{nt/Pep}$ = 20–23 nt) as compared with Pal2, suggests that a duplex motif contains 5–6 base pairs. Various configurations of higher-order complexes are possible, of which two are drawn for a single strand in Figure 5A (left and central panels). Similar configurations are possible with duplexes as illustrated in Figure 5A (right panel).

Binding properties measured for the larger SL2-cSL2 duplex and for other strands do not contradict the model. The 27mer SL2-cSL2 duplex is predicted to carry five motifs (each containing 5–6 bp) and to be able to form 5 Pep/2 ONs complexes ($St_{Pep/ON}$ = 2.5) with a K_D in the same range as that measured for 16mer duplexes. Experimental data are consistent with this prediction ($St_{Pep/ON}$ = 2.7 ± 0.3; K_D = 0.33 ± 0.05 μM). The parameters measured for half-DLS, dPal2 and dRD differ from those discussed so far by nearly integer stoichiometries and weaker affinities. Although they are not as accurate as those measured for other ONs, affinities are undoubtedly weaker, suggesting that the peptide motif can recognize <5–6 nt, as illustrated in Figure 5B (left panel). Indeed, half-DLS is too short to contain two 5–6-nt motifs. Similarly, a stoichiometry of 2 for dPal2 and dRD would be consistent with a model in which each peptide coats at the maximum 8 nt (on average 4 nt per peptide E motif; Figure 5B, right panel), explaining its reduced affinity (0.9–1.2 μM). Although a multi-motif

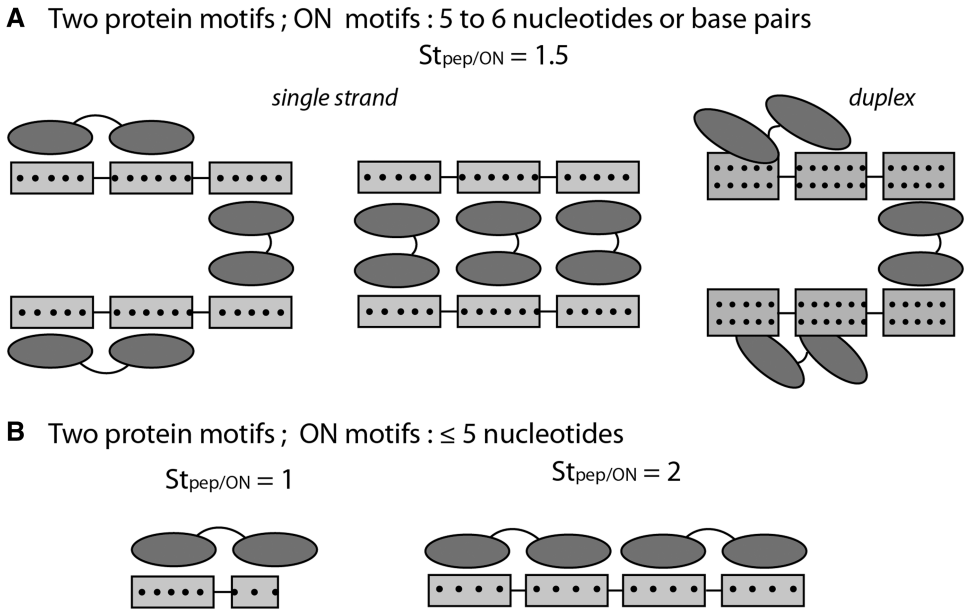

Figure 5. Model for the peptide E–ON interactions. (**A**) Two among the possible configurations for complexes formed of three peptides and two 16mer ribo-ON strands (left and central panels), valid also for duplexes (right panel): the peptide (dark grey) and ONs (light grey) contain two and three motifs, respectively. (**B**) Weaker binding may result from the presence of fewer negative charges in the ON motifs because of a smaller interface (half-DLS) or because of the more expanded deoxy-ON strand compared to the ribo-ON strand. Bridging (not drawn) cannot be excluded when stoichiometries are integers.

binding model that allows the bridging of ONs by peptide E was proposed based on non-integer $St_{Pep/ON}$ (16mer strand and duplexes), an integer $St_{Pep/ON}$ does not exclude the possibility of bridging (not drawn in Figure 5B). For example, $St_{Pep/ON} = 1$ if the two peptide motifs bind to the same ON, or if the two motifs in two peptides bridge two ONs. The mixed (stem and loop) composition of stem-loops, together with the structural and binding heterogeneity of SL2, make it difficult to relate structure with binding, but multi-motif binding and bridging is likely to apply in this case also. Altogether, our data suggest that with a few exceptions, peptide E maximizes ON coating, rather than searching for an appropriate sequence for getting the highest affinity.

SPR has been applied previously to the detailed analysis of nucleic acid binding by another nucleic acid chaperone, the HIV-1 nucleocapsid characterized by two highly folded zinc finger motifs (27,32). The data indicated the formation of higher-order complexes with an 8mer dON at high ON immobilization levels, whereas the same ON–nucleocapsid interaction showed a 1:1 stoichiometry at low immobilization levels, suggesting that stoichiometry depended on the ON density on the chip. An evaluation of the average distance between ONs in the dextran matrix indicates that the low ON density used in our experiments does not prevent bridging of ONs by the peptide. This separation was evaluated to be ~350–400 Å at immobilization levels in the range 20–45 RU, used in our study. As the dextran chains are not cross-linked and have an average length of 100 nm, this is more than twice the required bridging distances of a few hundred Ångströms. We also observe different $St_{Pep/ON}$ for different ONs, but at similar densities. We conclude that the formation of higher-order complexes is possible.

CONCLUSION

To our knowledge, this is the first characterization of the interaction of a disordered RNA-binding protein with ONs by SPR. Affinity data identify different modes of ON binding. Its sequence/structure-independent over-stoichiometric binding to strands and duplexes points to a largely non-specific interaction that may be representative of a nucleic acid coating activity. A more specific mode, possibly related to core chaperone activities, was observed with stem-loops, particularly SL2. Such a co-existence of both specific and non-specific binding, associated with different roles during the viral life cycle has already been described for the HIV-1 nucleocapsid chaperone (33). Stoichiometry data are consistent with a model in which two peptide E motifs recognize two nucleic acid motifs, allowing the formation of higher-order complexes if these are located on different ONs. The presence of two motifs on the peptide is consistent with the fact that it is composed of two basic domains of core. The ability of peptide E to bridge nucleic acid fragments is unlikely to be restricted to strands and duplexes (which served to develop the model) and has functional significance for nucleic acid chaperone activities such as dimerization or annealing, in bringing nucleic acid stretches together. It has been largely shown that structured RNA-binding proteins are modular and that this modularity is relevant to function [for review, see (34,35)]. The modular binding mode demonstrated for structured RNA-binding proteins is likely to apply also to the disordered HCV core.

SUPPLEMENTARY DATA

Supplementary Data are available at NAR Online.

ACKNOWLEDGEMENTS

The authors thank H. de Rocquigny for peptide synthesis.

FUNDING

French National Agency against AIDS (ANRS); 'Agence Nationale de La Recherche' (ANR blanc Femtostack); 'Centre National de la Recherche Scientifique' (CNRS); University of Strasbourg (UdS). Funding for open access charge: Waived by Oxford University Press.

Conflict of interest statement. None declared.

REFERENCES

1. Appel,N., Schaller,T., Penin,F. and Bartenschlager,R. (2006) From structure to function: new insights into hepatitis C virus RNA replication. *J. Biol. Chem.*, **281**, 9833–9836.
2. Dubuisson,J. (2007) Hepatitis C virus proteins. *World J. Gastroenterol.*, **13**, 2406–2415.
3. Sharma,S.D. (2010) Hepatitis C virus: molecular biology & current therapeutic options. *Indian J. Med. Res.*, **131**, 17–34.
4. Polyak,S.J., Klein,K.C., Shoji,I., Miyamura,T. and Lingappa,J.R. (2006) Assemble and interact: pleiotropic functions of the HCV core protein. In: Tan,S.L. (ed.), *Hepatitis C Viruses: Genomes and Molecular Biology*, Chapter 3. Horizon Bioscience, Norfolk, UK.
5. Irshad,M. and Dhar,I. (2006) Hepatitis C virus core protein: an update on its molecular biology, cellular functions and clinical implications. *Med. Princ. Pract.*, **15**, 405–416.
6. Hourioux,C., Ait-Goughoulte,M., Patient,R., Fouquenet,D., Arcanger-Doudet,F., Brand,D., Martin,A. and Roingeard,P. (2007) Core protein domains involved in hepatitis C virus-like particle assembly and budding at the endoplasmic reticulum membrane. *Cell. Microbiol.*, **9**, 1014–1027.
7. Jones,D.M. and McLauchlan,J. (2010) Hepatitis C virus: assembly and release of virus particles. *J. Biol. Chem.*, **285**, 22733–22739.
8. Ivanyi-Nagy,R., Lavergne,J.P., Gabus,C., Ficheux,D. and Darlix,J.L. (2008) RNA chaperoning and intrinsic disorder in the core proteins of Flaviviridae. *Nucleic Acids Res.*, **36**, 712–725.
9. Cristofari,G., Ivanyi-Nagy,R., Gabus,C., Boulant,S., Lavergne,J.P., Penin,F. and Darlix,J.L. (2004) The hepatitis C virus Core protein is a potent nucleic acid chaperone that directs dimerization of the viral (+) strand RNA *in vitro*. *Nucleic Acids Res.*, **32**, 2623–2631.
10. Ivanyi-Nagy,R., Kanevsky,I., Gabus,C., Lavergne,J.P., Ficheux,D., Penin,F., Fossé,P. and Darlix,J.L. (2006) Analysis of hepatitis C virus RNA dimerization and core-RNA interactions. *Nucleic Acids Res.*, **34**, 2618–2633.
11. Sharma,K., Didier,P., Darlix,J.L., de Rocquigny,H., Bensikaddour,H., Lavergne,J.P., Pénin,F., Lessinger,J.M. and Mély,Y. (2010) Kinetic analysis of the nucleic acid chaperone activity of the hepatitis C virus core protein. *Nucleic Acids Res.*, **38**, 3632–3642.
12. Sharma,K.K., de Rocquigny,H., Darlix,J.L., Lavergne,J.P., Pénin,F., Lessinger,J.M. and Mély,Y. (2012) Analysis of the RNA chaperoning activity of the hepatitis C virus core protein on the conserved 3'X region of the viral genome. *Nucleic Acids Res.*, **40**, 2540–2553.
13. Slutsky,M. and Mirny,L.A. (2004) Kinetics of protein-DNA interaction: facilitated target location in sequence-dependent potential. *Biophys. J.*, **87**, 4021–4035.
14. Halford,S.E. (2009) An end to 40 years of mistakes in DNA-protein association kinetics? *Biochem. Soc. Trans.*, **37**, 343–348.
15. Kolomeisky,A.B. (2011) Physics of protein-DNA interactions: mechanisms of facilitated target search. *Phys. Chem. Chem. Phys.*, **13**, 2088–2095.
16. Doetsch,M., Schroeder,R. and Fürtig,B. (2011) Transient RNA–protein interactions in RNA folding. *FEBS J.*, **278**, 1634–1642.
17. Duvignaud,J.B., Savard,C., Fromentin,R., Majeau,N., Leclerc,D. and Gagné,S.M. (2009) Structure and dynamics of the N-terminal half of hepatitis C virus core protein: an intrinsically unstructured protein. *Biochem. Biophys. Res. Commun.*, **378**, 27–31.
18. Ivanyi-Nagy,R. and Darlix,J.L. (2010) Intrinsic disorder in the core proteins of flaviviruses. *Protein Pept. Lett.*, **17**, 1019–1025.
19. Fink,A.L. (2005) Natively unfolded proteins. *Curr. Opin. Struct. Biol.*, **15**, 35–41.
20. Tompa,P. and Csermely,P. (2004) The role of structural disorder in the function of RNA and protein chaperones. *FASEB J.*, **18**, 1169–1175.
21. Shetty,S., Kim,S., Shimakami,T., Lemon,S.M. and Mihailescu,M.R. (2010) Hepatitis C virus genomic RNA dimerization is mediated via a kissing complex intermediate. *RNA*, **16**, 913–25.
22. Katsamba,P.S., Park,S. and Laird-Offringa,I.A. (2002) Kinetic studies of RNA-protein interactions using surface plasmon resonance. *Methods*, **26**, 95–104.
23. von der Haar,T. and McCarthy,J.E. (2003) Studying the assembly of multicomponent protein and ribonucleoprotein complexes using surface plasmon resonance. *Methods*, **29**, 167–174.
24. Majka,J. and Speck,C. (2007) Analysis of protein-DNA interactions using surface plasmon resonance. *Adv. Biochem. Eng. Biotechnol.*, **104**, 13–36.
25. Lin,S., Lee,A.S.-Y., Lin,C.-C. and Lee,C.-K. (2006) Determination of Binding Constant and Stoichiometry for Antibody-Antigen Interaction with Surface Plasmon Resonance. *Current Proteomics*, **3**, 271–282.
26. Stephen,A.G., Datta,S.A., Worthy,K.M., Bindu,L., Fivash,M.J., Turner,K.B., Fabris,D., Rein,A. and Fisher,R.J. (2007) Measuring the binding stoichiometry of HIV-1 Gag to very-low-density oligonucleotide surfaces using surface plasmon resonance spectroscopy. *J. Biomol Tech.*, **18**, 259–266.
27. Fisher,R.J., Fivash,M.J., Stephen,A.G., Hagan,N.A., Shenoy,S.R., Medaglia,M.V., Smith,L.R., Worthy,K.M., Simpson,J.T., Shoemaker,R. *et al.* (2006) Complex interactions of HIV-1 nucleocapsid protein with oligonucleotides. *Nucleic Acids Res.*, **34**, 472–484.
28. Myszka,D.G. (1999) Improving biosensor analysis. *J. Mol. Recognit.*, **12**, 279–284.
29. Hugo,N., Weidenhaupt,M., Beukes,M., Xu,B., Janson,J.C., Vernet,T. and Altschuh,D. (2003) VL position 34 is a key determinant for the engineering of stable antibodies with fast dissociation rates. *Protein Eng.*, **16**, 381–386.
30. Palau,W., Masante,C., Ventura,M. and Di Primo,C. (2013) Direct evidence for RNA-RNA interactions at the 3' end of the Hepatitis C virus genome using surface plasmon resonance. *RNA*, **19**, 982–991.
31. Di Primo,C. and Lebars,I. (2007) Determination of refractive index increment ratios for protein-nucleic acid complexes by surface plasmon resonance. *Anal. Biochem.*, **368**, 148–155.
32. Fisher,R.J., Rein,A., Fivash,M., Urbaneja,M.A., Casas-Finet,J.R., Medaglia,M. and Henderson,L.E. (1998) Sequence-specific binding of human immunodeficiency virus type 1 nucleocapsid protein to short oligonucleotides. *J. Virol.*, **72**, 1902–1909.
33. Darlix,J.L., Godet,J., Ivanyi-Nagy,R., Fossé,P., Mauffret,O. and Mély,Y. (2011) Flexible nature and specific functions of the HIV-1 nucleocapsid protein. *J. Mol. Biol.*, **410**, 565–581.
34. Shamoo,Y., Abdul-Manan,N. and Williams,K.R. (1995) Multiple RNA binding domains (RBDs) just don't add up. *Nucleic Acids Res.*, **23**, 725–728.
35. Lunde,B.M., Moore,C. and Varani,G. (2007) RNA-binding proteins:modular design for efficient function. *Nat. Rev. Mol. Cell Biol.*, **8**, 479–490.